MNRAS **476,** 933–942 (2018)
Advance Access publication 2018 January 31
doi:10.1093/mnras/sty257

Periodic optical variability and debris accretion in white dwarfs: a test for a causal connection*

Na'ama Hallakoun,[1,2★] Dan Maoz,[1] Eric Agol,[3] Warren R. Brown,[4] Patrick Dufour,[5] Jay Farihi,[6] Boris T. Gänsicke,[7] Mukremin Kilic,[8] Alekzander Kosakowski,[8] Abraham Loeb,[9] Tsevi Mazeh[1] and Fergal Mullally[10]

[1]*School of Physics and Astronomy, Tel-Aviv University, Tel-Aviv 6997801, Israel*
[2]*European Southern Observatory, Karl-Schwarzschild-Straße 2, D-85748 Garching, Germany*
[3]*Department of Astronomy, Box 351580, University of Washington, Seattle, WA 98195, USA*
[4]*Smithsonian Astrophysical Observatory, 60 Garden St, Cambridge, MA 02138, USA*
[5]*Institut de Recherche sur les Exoplanètes (iREx) and Département de physique, Université de Montréal, Montréal, QC H3C 3J7, Canada*
[6]*Department of Physics and Astronomy, University College London, London WC1E 6BT, UK*
[7]*Department of Physics, University of Warwick, Coventry CV4 7AL, UK*
[8]*Department of Physics and Astronomy, University of Oklahoma, 440 W. Brooks St, Norman, OK 73019, USA*
[9]*Department of Astronomy, Harvard University, 60 Garden St, Cambridge, MA 02138, USA*
[10]*SETI Institute/NASA Ames Research Center, Moffet Field, CA 94035, USA*

Accepted 2018 January 28. Received 2018 January 25; in original form 2017 November 28

ABSTRACT

Recent *Kepler* photometry has revealed that about half of white dwarfs (WDs) have periodic, low-level ($\sim 10^{-4} - 10^{-3}$), optical variations. *Hubble Space Telescope* (*HST*) ultraviolet spectroscopy has shown that up to about one half of WDs are actively accreting rocky planetary debris, as evidenced by the presence of photospheric metal absorption lines. We have obtained *HST* ultraviolet spectra of seven WDs that have been monitored for periodic variations, to test the hypothesis that these two phenomena are causally connected, i.e. that the optical periodic modulation is caused by WD rotation coupled with an inhomogeneous surface distribution of accreted metals. We detect photospheric metals in four out of the seven WDs. However, we find no significant correspondence between the existence of optical periodic variability and the detection of photospheric ultraviolet absorption lines. Thus, the null hypothesis stands, that the two phenomena are not directly related. Some other source of WD surface inhomogeneity, perhaps related to magnetic field strength, combined with the WD rotation, or alternatively effects due to close binary companions, may be behind the observed optical modulation. We report the marginal detection of molecular hydrogen in WD J1949+4734, only the fourth known WD with detected H_2 lines. We also re-classify J1926+4219 as a carbon-rich He-sdO subdwarf.

Key words: accretion, accretion discs – techniques: spectroscopic – stars: atmospheres – stars: variables: general – white dwarfs – ultraviolet: planetary systems.

1 INTRODUCTION

Over 95 per cent of all stars end their lives as white dwarfs (WDs; Althaus et al. 2010). The observed properties of WDs thus hold the keys to numerous questions in diverse astronomical fields, from gravitational wave sources, through Type-Ia supernova progenitors, to the fate of planetary systems, to name a few. Studies have shown that many WDs accrete the debris of their former planetary systems (e.g. Jura 2003; Zuckerman et al. 2003, 2010). This has emerged in parallel to the realization that planets and planetary systems are common around all stars (e.g. Winn & Fabrycky 2015; Shvartzvald et al. 2016). WD debris accretion is sometimes evidenced in the discs detected around some WDs within the tidal disruption radius for typical asteroid densities. The discs appear as infrared-excess dust emission (e.g. Kilic et al. 2006), or as optical emission lines from gas (e.g. Manser et al. 2016). However, the most frequent manifestation of debris accretion is the photospheric ultraviolet

* Based on observations made with the NASA/ESA *Hubble Space Telescope*, obtained at the Space Telescope Science Institute, which is operated by the Association of Universities for Research in Astronomy, Inc., under NASA contract NAS 5-26555. These observations are associated with programmes 14082 (PI: Maoz), 11526 (PI: Green), and 14076 (PI: Gänsicke).

⋆E-mail: naama@wise.tau.ac.il

(UV) metal absorption lines (typically Si, but sometimes C and other elements) found in ≈30–50 per cent of all WDs observed with the Cosmic Origins Spectrograph (COS) of the *Hubble Space Telescope* (*HST*) (Gänsicke et al. 2012; Koester, Gänsicke & Farihi 2014).

The sinking time-scales in the strong surface gravity of most WDs are relatively short. For example, in hydrogen-dominated-atmosphere (DA) WDs with effective temperatures between 12 000 K and 25 000 K, heavy elements would disappear from the WD atmosphere within weeks or less (Koester & Wilken 2006; Koester 2009). Thus, the presence of the metal lines indicates ongoing accretion of rocky material in at least 30 per cent of all WDs (Koester et al. 2014). The implied accretion rates are in the range $\sim 10^5$–10^8 g s^{-1} (Koester et al. 2014). Furthermore, the *HST* data have permitted detailed composition analyses, showing that the accreted material has a diverse make-up, but often a terrestrial-mantle-like composition (Gänsicke et al. 2012), and sometimes even indications of large amounts of water (Farihi, Gänsicke & Koester 2013). Debris-accreting WDs have thus opened a new window to study the properties of planetary material and its post-main-sequence fate (e.g. Xu et al. 2017).

The original *Kepler* mission (Borucki et al. 2010) monitored more than 150 000 stars in a 115 deg^2 region for about 4 yr, mainly in pursuit of stellar transits by Earth-like planets. Although the mission has focused primarily on main-sequence stars, a couple of dozen WDs were also observed, with unprecedented photometric precision. These WDs were included in the *Kepler* sample as a part of the astroseismology survey (Østensen et al. 2010). Although the survey was aimed at pulsating compact objects (i.e. WDs and hot subdwarfs), WDs known to be outside of the instability strip, along with other WD candidates within the *Kepler* field, were also included in the sample. However, none of the observed WDs turned out to be pulsating (Østensen et al. 2011; Doyle et al. 2017). Maoz, Mazeh & McQuillan (2015) analysed the *Kepler* time series for 14 WDs in the *Kepler* data base, and found periodic photometric modulations in seven of them. The variation periods were of order hours to 10 d, with amplitudes of order 10^{-4}–10^{-3}, much lower than could have been detected with pre-*Kepler* technology.[1]

In individual cases of these WDs, the observed modulation could possibly be explained by the effects of companions – e.g. beaming (Zucker, Mazeh & Alexander 2007) due to reflex motion caused by a compact companion (although such close double degenerates are rare; Maoz & Hallakoun 2017; Maoz, Hallakoun & Badenes 2018), or reflection/re-radiation by a heated giant planet (no planets around WDs have yet been discovered; Fulton et al. 2014) or a brown dwarf companion (although no more than ∼2 per cent of WDs have brown dwarf companions; Girven et al. 2011; Steele et al. 2011). However, the high occurrence rate of the modulation, and the typical periods, both suggest WD rotation (e.g. Hermes et al. 2017) as the cause of the observed modulation. Furthermore, the fully radiative atmospheres of the warm WDs in the *Kepler* sample argue also against variations caused by long-lived star spots, which are associated with photospheric convection that sets in only in cooler atmospheres (Brinkworth et al. 2005; Tremblay et al. 2015). Finally, the extremely high magnetic fields required for magnetic dichroism (Angel, Borra & Landstreet 1981) make it unlikely that in more than one of the WDs the modulation is due to strong inhomogeneous surface magnetic fields. Instead, Maoz et al. (2015) hypothesized that the optical-band low-level photometric modulation seen in one-half of WDs observed with *Kepler* could be associated with the previously mentioned photospheric metal pollution, that is seen in one-half of WDs observed in the UV with the *HST* (Koester et al. 2014). Slightly inhomogeneous surface coverage of the accreted material (e.g. due to moderate magnetic fields) would lead to inhomogenous UV absorption. Optical fluorescence of the absorbed UV photons (Pinto & Eastman 2000), combined with the WD rotation, could then potentially produce the observed levels and periods of optical modulation.

To test this hypothesis, we have obtained UV spectra of both variable and non-variable WDs. If our hypothesis is correct, there will be a one-to-one 'match' between the WDs with/without modulations and the WDs with/without photospheric metal absorption lines.

2 OBSERVATIONS

2.1 Sample selection

We have obtained UV spectra of seven WDs that have been monitored for low-level variability with a good signal-to-noise ratio (S/N): three WDs that show clear periodic modulations in the *Kepler* data (or elsewhere), and four that do not, with upper limits on any periodic variability at amplitude levels below 100 ppm (i.e. 10^{-4}). To ensure sufficient S/N ($\gtrsim$10 per resolution element), only WDs with a high expected UV signal were chosen. These were WDs with either a UV detection with *GALEX* at ≈1550 Å, or a visual magnitude extrapolated to the UV based on an effective temperature estimate such that desired S/N was expected. Additional selection criteria for all seven WDs were: effective temperatures $T_{\rm eff} < 36\,000$ K, to avoid WDs in which radiative levitation is dominant; and surface gravities $7.5 < \log g < 8.5$, to include only WDs of the kind whose UV metal pollution has been studied.

All four non-varying WDs were chosen from the *Kepler* sample, since no other ∼100 ppm sensitivity level WD light curves exist. The variable WDs include two targets from *Kepler*, and one additional target from the Pro-Am White Dwarf Monitoring (PAWM) survey[2] (WD 2359−434, see Section 3.2.3 below; Gary et al. 2013).

Our original sample included two additional objects: a non-varying WD (WD J1940+4240, see Section 3.3.1), that turned out to be much cooler than previously estimated, resulting in no signal in the *HST* far-UV (FUV) data; and a variable object (J1926+4219, see Section 3.3.2) that had been misclassified as a WD, and turned

[1] *Kepler* data for an additional 13 WDs were analysed by Doyle et al. (2017). None of these 13 light curves show any periodic variability. From the total of 18 WDs with *Kepler* data examined by Doyle et al. (2017), out of which five were included in the Maoz et al. (2015) sample, only one (KIC 11604781, or WD J1914+4936) displayed periodic variations, in agreement with Maoz et al. (2015). An additional WD (KIC 8682822, or WD J1917+4452) classified as possibly variable at the low 60 ppm level by Maoz et al. (2015), was found to be non-variable by Doyle et al. (2017). After a re-analysis of its light curve we agree with Doyle et al. (2017) and consider this WD non-variable, at the level of $\lesssim$ 60 ppm. Although, from the analysis of Doyle et al. (2017) it might appear that the actual fraction of periodically variable WDs is lower than reported by Maoz et al. (2015), all of the additional 13 WDs analysed by Doyle et al. (2017) have light curves of lower S/N, with upper limits of several hundred ppm on the variability – and are hence less sensitive by an order of magnitude to the variations detected by Maoz et al. (2015). Many hundreds of additional WDs have been monitored in *Kepler*'s *K2* continuation campaigns, albeit with lower photometric precision and over few-month-long observing periods.

[2] http://brucegary.net/WDE/

Table 1. Original sample: names and J2000 coordinates.

Name	KIC	RA	Dec
WD J1855+4207	6669882	18:55:46.033	+42:07:04.43
WD J1857+4909	11337598	18:57:47.150	+49:09:38.60
WD J1909+4717	10198116	19:09:59.347	+47:17:10.00
WD J1919+3958	4829241	19:19:27.685	+39:58:39.71
J1926+4219	6862653	19:26:46.011	+42:19:35.32
WD J1940+4240	7129927	19:40:59.367	+42:40:31.30
WD 1942+499	11822535	19:43:43.686	+50:04:37.80
WD J1949+4734	10420021	19:49:14.579	+47:34:45.98
WD 2359−434	–	00:02:10.766	−43:09:56.02

out to be a carbon-rich helium-dominated subdwarf. We exclude both of them from our analysis. Table 1 lists the names, including the *Kepler* Input Catalogue (KIC) designation, and coordinates of all the nine objects from our original sample. In this paper, we have adopted the naming convention of WD Jhh:mm±dd:mm based on the J2000 coordinates, unless a legacy B1950 WD hh:mm±dd:m name was already in use (i.e. WD 1942+499 and WD 2359−434).

The initial choice of nine WDs should have permitted, in principle, to significantly reject the null hypothesis that optical modulations and UV metal pollution are unrelated. Since the probability for any WD to display each effect alone is ≈50 per cent (Koester et al. 2014; Maoz et al. 2015), the chance probability for n matches would be 2^{-n}. Even if in two of the nine WDs there could be a mismatch (due to a different cause for the modulation, such as rotation plus magnetic dichroism, or beaming caused by the presence of a close companion), this would still leave seven WDs with a match between the two effects. The chance probability for seven matches would be $2^{-7} < 1$ per cent, and thus seven or more matches would firmly reject the null hypothesis.

2.2 *HST* observations

We obtained (*HST* programme 14082, PI: Maoz) FUV spectra with COS (Green et al. 2012) for six WDs and the misidentified subdwarf, using the G130M grating with a central wavelength of 1291 Å, which covers the wavelength range 1130–1435 Å, excluding a gap between the two detector segments, at 1278–1288 Å. The dispersion is 0.01 Å pixel^{-1}. Each exposure was split into four sub-exposures, slightly dithered in the dispersion direction, in order to eliminate the COS MCD fixed-pattern noise. Four of the WDs were observed for one *HST* orbit, while the fainter remaining three were observed for two orbits, in order to achieve a higher S/N. The observational setup is similar to that used by Koester et al. (2014), Farihi et al. (2013), Gänsicke et al. (2012) in their search for UV metal absorption lines in 85 WDs.

We retrieved archival data for two additional WDs: WD 1942+499, for which a COS/FUV spectrum using a similar configuration was available from *HST* programme 11526 (PI: Green); and WD 2359−434, for which a Space Telescope Imaging Spectrograph (STIS) near-UV (NUV) spectrum was available from *HST* programme 14076 (PI: Gänsicke). The STIS observations were performed using the G230L grating with a central wavelength of 2376 Å, which covers the wavelength range 1600–3150 Å, with a dispersion of about 1.5 Å pixel^{-1}. All spectra underwent standard reduction by the appropriate *HST* pipeline.

2.3 Radial velocity measurements

In order to rule out the presence of a massive WD or M-dwarf companion as a cause for the modulation in the variable WDs, and in general to examine the possibility of binarity in the sample, we have obtained ground-based spectroscopic observations, as described below. These observations are analysed and summarized in Section 4.

We used the Dual Imaging Spectrograph (DIS) mounted on the ARC 3.5-m telescope at Apache Point Observatory (APO) in New Mexico on the nights of 2017 April 30 and 2017 June 17. We obtained a total of 27 epochs of the seven northern objects in our sample, with an exposure time varying between 300 and 1200 s. We used the 1200 lines mm^{-1} gratings centred around 4380 and 6500 Å, and a 0.9 arcsec slit, covering the range 3750–5010 Å with 0.62 Å pix^{-1} dispersion in the blue channel, and 5920–7100 Å with 0.56 Å pix^{-1} dispersion in the red channel. To improve our wavelength calibration, a HeNeAr comparison lamp spectrum was obtained after each observation. The weather was clear on both nights, yielding an S/N of ≈3–5 for the first night and ≈2–15 for the second night. Standard IRAF packages were used to perform bias correction, flat-fielding, spectrum extraction, and wavelength calibration. Flux calibration was completed using standard IRAF packages with the ESO spectrophotometric standard star BD +33d2642.

Eight additional epochs of five of the northern objects were obtained using the 6.5-m MMT telescope Blue Channel Spectrograph on Mt. Hopkins, Arizona, on the nights of 2017 June 24–26. We used the 832 lines mm^{-1} grating in the second order and a 1 arcsec slit, covering the range 3570–4510 Å with 0.36 Å pix^{-1} dispersion and a 1 Å spectral resolution. The exposure time varied between 75 and 720 s. Wavelength calibration was performed with arc lamp spectra obtained immediately after each exposure. Because the targets are relatively bright, the observations could be made during poor seeing and/or some cloud cover. The spectra have an S/N per resolution element between 20 and 50 in the continuum.

3 RESULTS AND ANALYSIS

Figs 1–7 show the *HST* pipeline-reduced spectra for each of the seven WDs in the observed sample. We have visually searched each spectrum for absorption lines. To determine the nature of the lines (photospheric or interstellar), we have fitted each spectrum with a synthetic WD model generated with the spectral synthesis program SYNSPEC (version 50; Hubeny & Lanz 2011), based on model atmospheres created by the TLUSTY program (version 205; Hubeny 1988; Hubeny & Lanz 1995, 2017a). TLUSTY produces one-dimensional, horizontally homogeneous, plane-parallel model atmospheres in hydrostatic equilibrium. Following the moderately cool WD example of Hubeny & Lanz (2017b), we have assumed ML2-type convection with a mixing length of 0.6 of a pressure scale height. The models were computed in local thermodynamic equilibrium, using the Tremblay tables (Tremblay & Bergeron 2009) for hydrogen line broadening.

For each WD, the basic model atmosphere was computed with TLUSTY using the published effective temperature and surface gravity estimates, except in the case of WD J1949+4734 and J1926+4219, where the published values were inconsistent with the observations (see below). We then used SYNSPEC to produce various synthetic spectra with different Si and C abundances, in steps of 1 dex, for each element separately. Each model spectrum was convolved with the COS line spread function.[3] The model was then scaled and

[3] http://www.stsci.edu/hst/cos/performance/spectral_resolution

Table 2. WD properties – effective temperature ($T_{\rm eff}$), surface gravity ($\log g$), optical variability period (P), amplitude (A); and Si and C abundances relative to hydrogen, as determined from the model fits to the *HST* data. The 'Z?' column indicates detection of photospheric metal lines. The 'Hyp?' column indicates whether the WD matches our experiment's hypothesis, that optical variability and debris accretion are related. See Section 3 for further details.

Name	Spectral type	$T_{\rm eff}$ (kK)	$\log g$	P (h)	A (ppm)	$\log({\rm Si/H})$	$\log({\rm C/H})$	Z?	Hyp?	Notes	Ref.
Non-variable WDs:											
WD J1909+4717	DA	13.5	8.0	–	<70	-7.8 ± 0.2	<-8.0	+	–	1, 2	a, e
WD J1919+3958	DA	19.5	8.0	–	<50	<-9.0	<-8.5	–	+		a, e
WD 1942+499	DA	36	7.9	–	<20	-6.3 ± 0.3	<-8.5	+	–	3	b, e
WD J1949+4734	DA	12.8	7.8	–	<50	<-8.0	-6.7 ± 0.3	+	–	2, 4	c, e
Periodically variable WDs:											
WD J1855+4207	DA	30.5	7.4	8.81 ± 0.22	800	-7.4 ± 0.2	-7.8 ± 0.2	+	+	3	b, e
WD J1857+4909	DA	22.8	8.6	$2.238\,72 \pm 0.000\,72$	300	<-8.5	<-8.5	–	–		b, e
WD 2359−434	DA	8.6	8.3	$2.694\,926 \pm 0.000\,073$	5 000	<-9.5	<-8.0	–	?	5, 6	d, f

Notes: (1) Tentative Si detection. (2) Low S/N. (3) Possible detection of circumstellar material. (4) H_2 detected. (5) NUV spectrum only. (6) $\log({\rm Mg/H}) < -10$.

References: $T_{\rm eff}$ and $\log g$ based on (a) Doyle et al. (2017), (b) Østensen et al. (2011), (c) this work (see text), (d) Giammichele, Bergeron & Dufour (2012). P and A based on (e) Maoz et al. (2015), or (f) Gary et al. (2013).

Doppler shifted to match the observed spectrum, using χ^2 minimization. Following a visual inspection of the observed spectrum and the various model spectra, we repeated the procedure using smaller steps of 0.2 dex, around the best-fitting abundance value. Finally, a combined model spectrum consisting of both Si and C with the matched abundances was created, convolved, shifted, and scaled to fit the observed spectrum, or to find the upper limits on metal abundances in the cases with no detection of either or both elements. We note that the various expected metal absorption line strengths depend strongly on both temperature and surface gravity, and therefore the levels of the abundance limits in the cases of non-detection vary among the WDs. The results, including the derived abundances, are summarized in Table 2. Figs 1–7 also show the model fits in selected regions. The absorption lines absent from the models are of interstellar origin (interstellar lines of C II, N I, O I, Si II, S II, and Fe II were detected), unless mentioned otherwise. The results for each WD are discussed in detail below.

In their *HST* survey of warm (17 000–27 000 K) DA-type WDs, Koester et al. (2014) detected photospheric metal absorption lines in 48 out of 85 WDs. All of these 48 WDs had Si lines in their atmosphere at abundances of $-8.5 \lesssim \log({\rm Si/H}) \lesssim -5$ (all abundances are by number). In 18 of them C lines were also detected ($-8.5 \lesssim \log({\rm C/H}) \lesssim -5.5$), and seven more had other metals as well (Mg, Al, P, S, Ca, Cr, Fe, or Ni). For reference, solar abundances are $\log({\rm Si/H}) = -4.49 \pm 0.03$ and $\log({\rm C/H}) = -3.57 \pm 0.05$, see Asplund et al. 2009. Since Si has always been detected when any metals are present in the sample of Koester et al. (2014), and because our upper limits on C in some WDs are comparable to the detected levels in other WDs, we will generally use the Si detection to determine if a WD has atmospheric metals or not. However, in WD J1949+4734 we have a clear detection of C at a relatively high abundance without Si (see Section 3.1.4 below), and we hence count it as a case of metal line detection.

3.1 Non-variable WDs

3.1.1 WD J1909+4717

Although this WD was observed for two *HST* orbits, the obtained COS/FUV spectrum is still rather noisy, with S/N ≈2 (or ≈3 after binning) at the relevant wavelength range. Nevertheless, we report a tentative detection of a photospheric Si II 1264.7 Å line, at an abundance of $\log({\rm Si/H}) \approx -7.8$ (see Fig. 1). Since under photospheric conditions the 1265 Å line is always stronger than the 1260 Å line (Koester et al. 2014), its presence, if real, indicates a photospheric origin. The photospheric origin is also independently supported by the weighted mean radial velocity (RV) measured from the Balmer lines in the optical spectra (see Section 4), that is consistent with the RV of the candidate photospheric absorption line (≈20 km s^{-1}). An interstellar 1260 Å Si II line, shifted by ≈40 km s^{-1} blue-ward compared to the photospheric line (see Fig. 1b), is also visible. If this is a true detection of a photospheric metal line, it contradicts the prediction from our hypothesis, of no photospheric metals in non-variable WDs.

The UV spectrum of this relatively cool DA shows the wide 1400 Å Lyα satellite line from collisions of H–H$^+$, common in DA WDs cooler than 20 000 K (Greenstein & Oke 1979; Wegner 1982; Koester et al. 1985; Nelan & Wegner 1985).

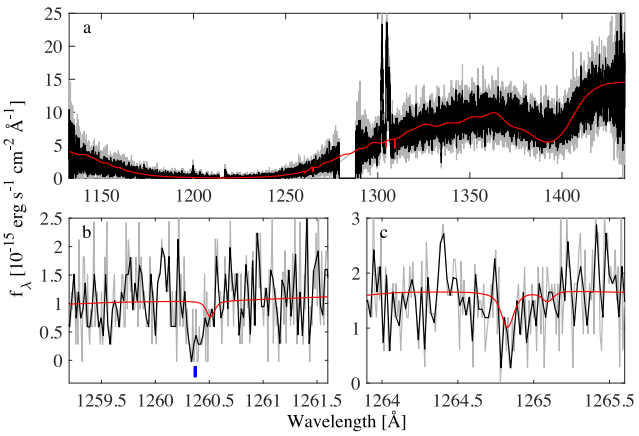

Figure 1. (a) *HST*/COS spectrum of WD J1909+4717 (unbinned, gray; binned every two data points, black) and model fit (red). Unmodelled absorption lines are of interstellar origin. Airglow of O I is visible around 1302 − 1306 Å. (b) Interstellar Si II 1260.4 Å line (blue tick) with a null or weak detection of the photospheric component of this line in the red wing of the interstellar line (red model). (c) Tentative detection of a photospheric Si II 1264.7 Å line.

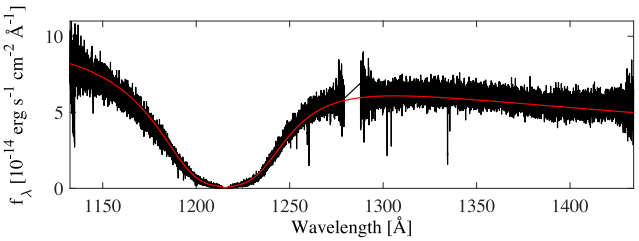

Figure 2. *HST*/COS spectrum of WD J1919+3958 (black) and model fit (red). Unmodelled absorption lines are of interstellar origin. No photospheric metal lines are detected within our sensitivity limits.

3.1.2 WD J1919+3958

No photospheric metal lines were detected in this WD (see Fig. 2), in accord with expectations from our hypothesis.

3.1.3 WD 1942+499

Since for this WD we use archival data obtained in 2010, in our modelling we have used Lifetime Position 1 of the COS line spread function, as opposed to Lifetime Position 3 used for the other COS observations. Si absorption lines from excited states that cannot have originated in the interstellar medium (Si III and Si IV) are detected in the COS/FUV spectrum (see Fig. 3), with our modelling indicating an abundance of $\log(\mathrm{Si/H}) \approx -6.3$. The RV estimated from the Si lines is consistent with the Balmer-line RV measured from the optical spectra, supporting the case for the photospheric origin of these absorption lines. Based on the lack of C II or C III absorption lines in the spectrum, we were able to constrain the C abundance to $\log(\mathrm{C/H}) < -8.5$. Nevertheless, in a previous study by Lallement et al. (2011) of the same COS data along with

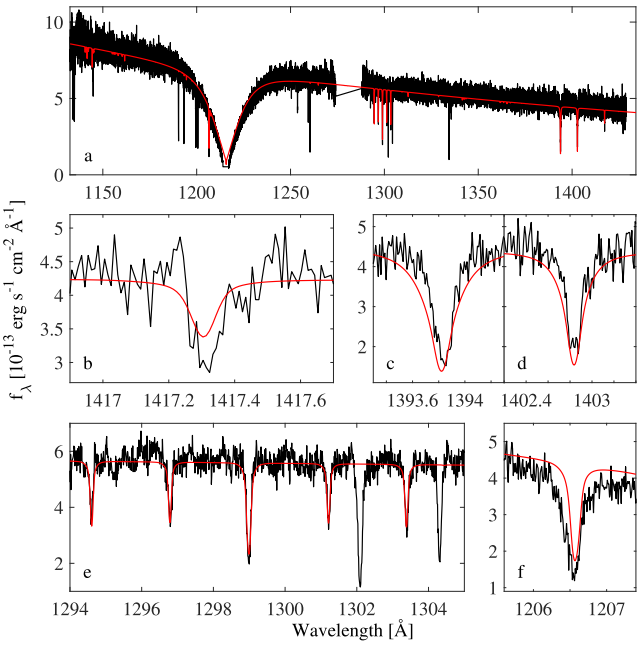

Figure 3. (a) *HST*/COS spectrum of WD 1942+499 (black) and model fit (red). Unmodelled absorption lines are of interstellar origin. (b) Si III. (c)+(d) Si IV. (e) Si III. The two strong lines absent from the model are interstellar O I 1302.2 Å and Si II 1304.4 Å. (f) Si IV 1206.5 Å absorption line. Note the slight discrepancy between the model fit and the observed line, which may have an additional blue-shifted component, perhaps of circumstellar origin.

an additional G160M-grating spectrum (covering the wavelength range 1400–1750 Å), C IV 1548 and 1551 Å absorption lines were detected, at an abundance of $\log(\mathrm{C/H}) \sim -7.6$. These lines may have a slight blue-shift relative to that of photospheric lines, but the shift is also consistent with zero within the measurement error (Barstow et al. 2010; Lallement et al. 2011). These authors also note a discrepancy in the Si abundance, as measured from the Si III ($\log(\mathrm{Si/H}) \sim -6.0$) and Si IV ($\log(\mathrm{Si/H}) \sim -6.7$) lines. Lallement et al. (2011) have suggested that the high-ionization absorption lines (Si IV, C IV, and N V, which is marginally detected) originate from circumstellar material surrounding the WD, and not from the photosphere. If these lines are circumstellar, then it is puzzling that they are not blue-shifted by ∼25–30 km s^{-1} relative to the photospheric Balmer lines, which undergo gravitational redshift. Indeed, in Debes et al. (2012) a claimed circumstellar Ca II line component in WD 1124−293 is blue-shifted by 30 km s^{-1} relative to the main photospheric component, as one would expect. In the present case, this would suggest that either the circumstellar material is in radial infall at roughly such a velocity, or that the material is only slightly above the photosphere, such that the lines undergo a similar gravitational redshift (a similar phenomenon is presented and discussed below, Section 3.2.1, for WD J1855+4207). Even if the high-ionization absorption lines do have a circumstellar origin, the Si III lines (and possibly part of the Si IV material; see Fig. 3f) are consistent with a photospheric model fit. Thus, although some of the material might be circumstellar, metals are present also in the WD photosphere.

Metals from a past accretion event can be supported in the atmospheres of hot DAs such as this one ($T_{\rm eff} \approx 36\,000$ K) by radiative levitation, leaving enough time for the metal distribution to become homogeneous, through transverse diffusion, over the WD surface. If so, the Si detection in a non-variable WD does not necessarily contradict the expectation from our hypothesis. However, the detected Si abundance is higher than expected from radiative levitation (Chayer et al. 1995), and therefore cannot be explained solely by a past accretion event. We thus count this case as a mismatch to our hypothesis.

3.1.4 WD J1949+4734

Two *HST* orbits were spent on this WD. Despite the rather low S/N of the obtained COS/FUV spectrum, a pair of 1334/35 C II absorption lines at an abundance of $\log(\mathrm{C/H}) \approx -6.7$ are clearly detected (see Fig. 4). The photospheric origin of these lines is established in this case by the detection of an interstellar 1334 Å C II line, shifted blue-ward by ≈50 km s^{-1} compared to the photospheric line, and the RV consistency with the optical Balmer lines.

Although Østensen et al. (2011) estimated $T_{\rm eff} \approx 16\,200$ K and $\log g \approx 7.8$ based on the optical spectrum of this WD, our fit to the UV spectrum suggests a significantly lower effective temperature of ≈12 750 K. To find the best-fitting model, we varied the $T_{\rm eff}$ around the value estimated from the spectral energy distribution (SED), until a sufficient fit was achieved. Similarly to WD J1909+4717 (see Section 3.1.1), this WD also shows the wide 1400 Å Ly α satellite line from collisions of H–H$^+$. In addition, several molecular hydrogen lines are marginally detected in the WD rest frame (see Fig. 4c), making it only the fourth known WD with molecular hydrogen (see Xu et al. 2013 for the first three). This detection of H_2 is consistent with our lower effective temperature estimate for this WD (see Zuckerman et al. 2013 for the similar case of GD 31).

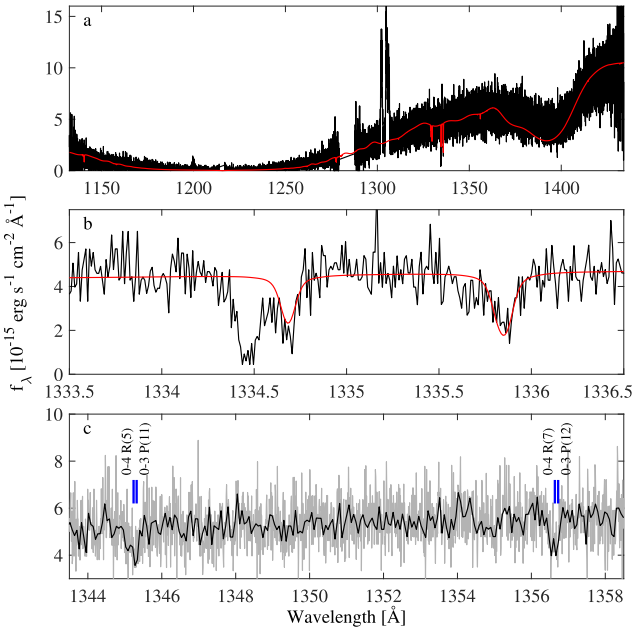

Figure 4. (a) *HST*/COS spectrum of WD J1949+4734 (black) and model fit (red). Unmodelled absorption lines are of interstellar origin. Airglow of O I is visible around 1302–1306 Å. (b) Interstellar and photospheric C II lines. (c) Molecular hydrogen absorption lines (unbinned spectrum, grey; binned every six data points, black). The blue ticks mark the theoretical wavelengths of the H_2 0–4 R(5), 0–3 P(11), 0–4 R(7), and 0–3 P(12) transitions (Abgrall et al. 1993; Xu et al. 2013), redshifted by ≈30 km s^{-1} to the WD rest frame.

Unless the presence of C in the atmosphere is the result of carbon dredge-up due to convection, this WD also constitutes a mismatch, counter to expectations from our hypothesis.

3.2 WDs with periodic modulations

3.2.1 WD J1855+4207

The COS/FUV spectrum of this WD (Fig. 5) shows photospheric absorption lines from C II, C III, Si III, and Si IV, in agreement with expectations from our hypothesis. The RV of the photospheric lines is broadly consistent with that measured from the low S/N optical spectra of this object. However, as in the case of WD 1942+499 (see Section 3.1.3), there is a discrepancy in the Si abundance measured from Si III and Si IV (see Fig. 5f, for example). High-ionization N V 1239 Å and 1243 Å absorption lines are also detected, close to the photospheric velocity (Fig. 5h and i). These N V lines cannot have originated from the ∼30 500 K photosphere, and require a temperature ≳80 000 K (Sion et al. 1998; Long & Gilliland 1999). Thus, WD J1855+4207 seems to have both photospheric and possibly infalling circumstellar metals, much like WD 1942+499.

The cases of WD J1855+4207 and WD 1942+499, discussed above, both of them hot $T_{\rm eff} > 30\,000$ K objects with indications of highly ionized circumstellar metals, in addition to the detected photospheric metals, are similar to the case of GD 394 (WD 2111+489), a $T_{\rm eff} \sim 35\,000$ K DA WD showing high-ionization C IV, N V, and P V lines, all approximately at the photospheric, gravitationally redshifted, velocity (Chayer et al. 2000; Wilson et al., in preparation). Closely related may be also the cases of SDSS 1228+1040 and WD 0843+516 (Koester et al. 2014), that show high-excitation Si IV absorption (but no N V), that is again slightly blue-shifted relative to the photospheric lines. This may be an emerging class of hot, polluted, WDs with signs of a circumstellar envelope that is either infalling, or perhaps levitated just above the photosphere.

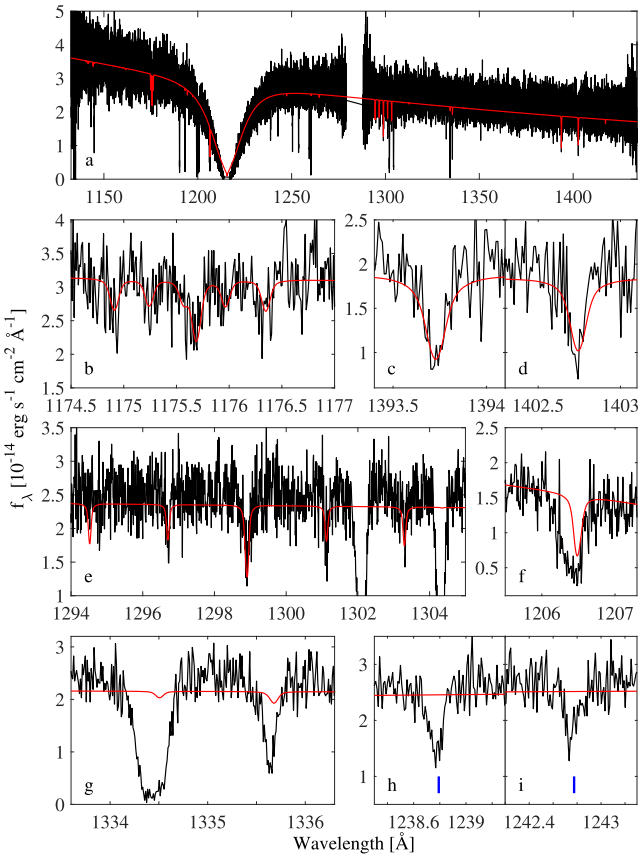

Figure 5. (a) *HST*/COS spectrum of WD J1855+4207 (black) and model fit (red). Unmodelled absorption lines are of interstellar origin. (b) C III. (c)+(d) Si IV. (e) Si III. The strong unmodelled lines are interstellar O I 1302.2 Å and Si II 1304.4 Å. (f) Si IV 1206.5 Å absorption line. Note the discrepancy between the model fit and the observed line, which has an additional blue-shifted component, possibly circumstellar. (g) Interstellar C II lines, with some small contribution from the photosphere. (h)+(i) N V absorption lines, possibly from circumstellar material (see Section 3.2.1). The blue ticks mark the WD rest frame.

3.2.2 WD J1857+4909

No photospheric metal absorption lines are detected (see Fig. 6), making this case a mismatch to expectations from our hypothesis.

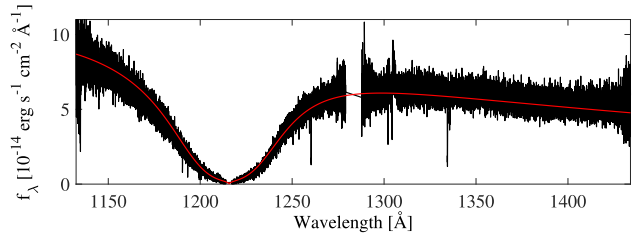

Figure 6. *HST*/COS spectrum of WD J1857+4909 (black) and model fit (red). Unmodelled absorption lines are of interstellar origin. Airglow of O I is visible around 1302 − 1306 Å. No photospheric metal lines are detected within our sensitivity limits.

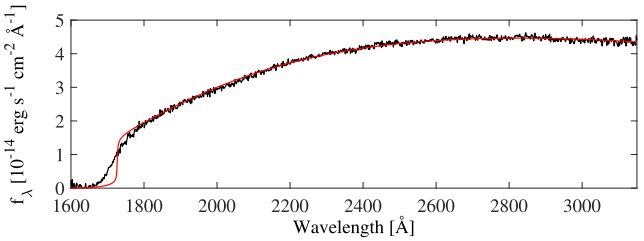

Figure 7. *HST*/STIS spectrum of WD 2359−434 (black) and model fit (red). No photospheric metal lines are detected within our sensitivity limits.

3.2.3 WD 2359−434

This WD was not part of the *Kepler* sample, but was discovered to have periodic modulations by the PAWM survey[4] (Gary et al. 2013). It was observed using STIS and we have therefore used the STIS line spread function[5] to broaden the model spectrum. We have also checked the NUV spectrum of this WD for the presence of Mg, since strong Mg I absorption lines are expected around 2800 and 2850 Å. Nevertheless, the spectrum shows no absorption lines of any kind (see Fig. 7 and Table 2), suggesting a mismatch to our hypothesis. However, since this WD is cool enough to be convective, the observed modulation could be the result of normal star spots (i.e. photospheric regions in which weak magnetic fields restrain the convective circulation, resulting in lower effective temperatures), as already proposed by Gary et al. (2013). We note that Gary et al. (2013)'s alternative explanation for the modulation, of reflection from an orbiting giant planet, is unlikely because the planet would be well within the tidal disruption radius for a gas planet around such a WD. Reflection from a cool ($\lesssim$1000 K) brown dwarf companion is a possibility (see Section 4).

The possibility of a moderate magnetic field in this WD was already raised by Koester et al. (1998), based on the flat Hα core shape, and confirmed by Aznar Cuadrado et al. (2004) and later by Kawka et al. (2007) using spectropolarimetry, yielding a longitudinal field strength of $\approx$3 kG. A mean field strength of $\approx$110 kG was measured by Koester et al. (2009), based on high-resolution spectroscopy. A recent study by Landstreet et al. (2017) monitored the variations in the magnetic field of this WD, based on the equivalent width of the Zeeman-split Hα line core, and found a period similar to the one of the photometric modulations detected by Gary et al. (2013). Landstreet et al. (2017) suggested that the variations observed in the Zeeman splitting are the result of the WD rotation combined with a non-axissymmetric multipolar magnetic field.

The UV spectrum of this DA shows the wide 1600 Å Lyα satellite line from collisions of H–H, common in DA WDs cooler than 13 500 K, as already observed by Koester et al. (1985). As can be seen in Fig. 7, our SYNSPEC model does not precisely reproduce the shape of the 1600 Å feature. This could be the result of suppressed convection as the result of the magnetic field (Tremblay et al. 2015; Gentile Fusillo et al. 2018), leading to a partially radiative atmosphere, that is inconsistent with the convective model that we use. However, if the magnetic field in this WD fully suppresses the convection on the WD surface, then it is hard to see how the star spots, presumably behind the optical modulations, could form. It is thus difficult to explain both the modulations and the spectral mismatch by means of the magnetic field.

[4] http://brucegary.net/WDE/WD2359-434/WD2359-434.htm
[5] http://www.stsci.edu/hst/stis/performance/spectral_resolution

3.3 Excluded objects

3.3.1 WD J1940+4240

The *Kepler* light curve of this WD shows no modulations down to $<$80 ppm (Maoz et al. 2015). Based on a poor atmospheric model fit, yielding $T_{\rm eff} \approx 23\,000$ K, Østensen et al. (2011) conjectured that this may be a DA+DA double WD. Unfortunately, our two-orbit-long COS observation resulted in almost no signal, as would have been expected from the recent, much cooler (and hence UV faint) $T_{\rm eff} \approx 9500$ K estimate of Doyle et al. (2017). As already noted, we exclude this WD from our analysis.

3.3.2 J1926+4219

This object was classified as a helium-dominated-atmosphere (DB) WD by Østensen et al. (2011). They estimated, based on line fits to the optical spectrum, $T_{\rm eff} \approx 16\,000$ K, but reported a poor fit. The *Kepler* light curve shows 14.16 ± 0.48 h, 500 ppm, periodic variations (Maoz et al. 2015). From its SED based on available photometry we estimated, prior to our observations, an effective temperature of $\approx$34 000 K, and a high S/N in the UV that we indeed obtained. Photospheric C II, C III, Si III, and Si IV absorption lines are detected in the FUV spectrum (see Fig. 8). However, during the modelling process we realized that this is in fact a helium-rich hot subdwarf (He-sdO). Using the TLUSTY-calculated non-local thermodynamic equilibrium (NLTE) grid of hot subdwarfs of Fontaine et al. (2014) to fit the co-added optical MMT spectrum we have acquired (Section 2.3), we estimate $T_{\rm eff} = 40\,300 \pm 210$ K, $\log g = 6.40 \pm 0.11$, and $\log({\rm He/H}) = 3.17 \pm 0.79$. We then use these parameters to create an NLTE TLUSTY model with C and Si, to fit the *HST* UV spectrum, and we find abundances of $\log({\rm C/He}) = -2.5 \pm 0.3$ and $\log({\rm Si/He}) = -4.6 \pm 0.2$. The high C abundance is consistent with the reported abundances of carbon-enhanced He-sdOs (Heber

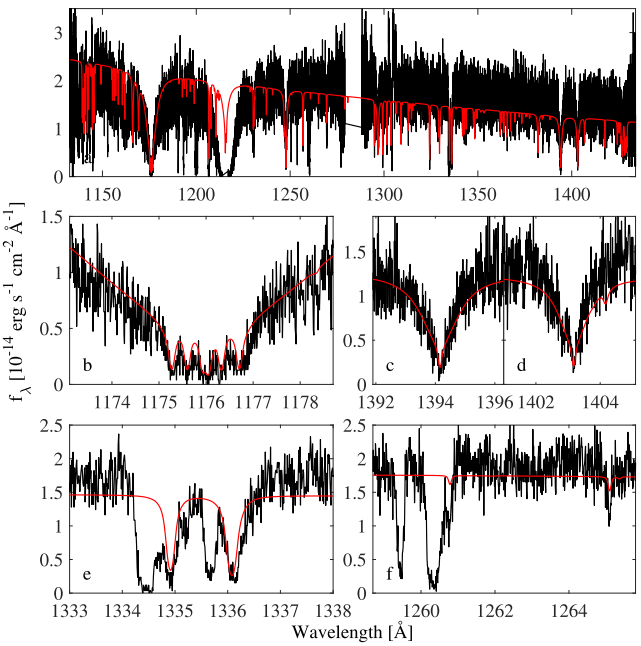

Figure 8. (a) *HST*/COS spectrum of the hot subdwarf J1926+4219 (black) and model fit (red). Unmodelled absorption lines are of interstellar origin. (b) C III. (c)+(d) Si IV. (e) Photospheric and unmodelled interstellar C II lines. (f) Photospheric Si II lines. The strong unmodelled lines are interstellar S II 1259.5 Å and Si II 1260.4 Å lines.

2016), although most of these reports have been for subdwarfs with a relatively higher effective temperature ($T_{\rm eff} > 43\,300$ K), while only two out of the 16 reported carbon-enhanced He-sdOs have $T_{\rm eff} \approx 40\,000$ K (like J1926+4219). Subdwarfs are evolved stars whose envelopes have been stripped, and therefore must have, or must have had in the past, a close companion. We discuss in Section 4 the constraints on the presence of a binary companion to this subdwarf.

4 A SEARCH FOR BINARY COMPANIONS

In order to test for a companion-induced (rather than rotation related) cause for the optical modulation of some of the WDs, we searched for the presence of companions using two approaches. First, we searched the SED for evidence of a cool stellar or substellar component. We examined on VizieR (Ochsenbein, Bauer & Marcout 2000) the available optical photometry of each of the WDs, and compared it to a Planck spectrum with a temperature of the atmospheric fit listed in Table 2, scaled to fit the optical-band photometry of the WD. We then searched for evidence of any near-infrared (NIR) excess at 3.6–8 μm as indicated by *Spitzer Space Telescope* IR Array Camera (IRAC) photometry available from the *Spitzer* Heritage Archive. For WD 1942+499 and WD 2359−434, we used cryogenic 4.5 and 8.0 μm images from the 'survey for planets and exozodiacal dust around WDs' (*Spitzer* programme 2313; Kuchner et al. 2004; Mullally et al. 2007). We used available 3.6 and 4.5 μm images from the warm 'Small *Spitzer Kepler* Survey' (Small SpiKeS; *Spitzer* programme 90100; Werner et al. 2012) for J1926+4219, and from SpiKeS (*Spitzer* programme 10067; Werner et al. 2013) for the remaining WDs. The photometry was performed using MOPEX (Makovoz & Marleau 2005) Point Response Function (PRF) fitting, corrected for the wavelength-dependent sensor sensitivity using the Rayleigh–Jeans tail correction factors provided by Reach et al. (2005). To quantify any detected excesses and estimate the detection limits for excesses, to each model Planck spectrum (representing the WD), we added an M-dwarf model (Allard 2016) of varying temperature, scaled according to the ratio of the surface areas of the WD and of an M-dwarf companion. The WD radii were estimated using the effective temperature and surface gravity listed in Table 2, and the theoretical WD cooling tracks of Fontaine, Brassard & Bergeron (2001).[6] We find no evidence for a companion warmer than ≈1000 K for all the WDs in our sample, except for the case of WD J1855+4207 in which the WD is too faint to be detected in the IR, and hence we can only exclude companions warmer than ≈2500 K. Similarly, we have no *Spitzer* detection for the hot subdwarf J1926+4219, and so can exclude only companions warmer than ≈4000 K.

Secondly, we have tested for massive stellar companions by searching for RV variations in the ground-based spectroscopic data, described in Section 2.3. We estimated the RV of each epoch by cross-correlating the observed spectrum with a synthetic model spectrum generated by TLUSTY using the atmospheric parameters that are listed in Table 2. The measured velocities were corrected to the barycentre rest frame using the EARTH_VEL_RON_VONDRAK MATLAB function of Ofek (2014). The RV uncertainty, estimated from the distribution of the RV differences between epochs of the same objects (scaled down by a factor $\sqrt{2}$ to account for the two measurement errors that enter a difference), was typically around ≈25 km s^{-1}, but could also be as large as ≈80 km s^{-1} in epochs with a low S/N. No significant RV variations are detected, within the limits of our sensitivity. We examine the implications of these RV variation limits for a putative binary companion for each of the periodically variable WDs in the sample.

For WD J1855+4207, with a primary mass of about 0.45 M$_\odot$ (based on the cooling tracks of Fontaine et al. 2001) and an orbital period of 8.8 h, the upper limit on any companion mass, M_2, is $M_2 \sin i \lesssim 0.20$ M$_\odot$, where i is the orbital inclination angle. The relatively low mass of this WD places it at the lower limit of single-star evolution (single stars that evolve into $\lesssim$0.45 M$_\odot$ WDs have not left the main sequence yet, e.g. Brown et al. 2016). Beaming modulation of the WD flux due to reflex motion caused by a massive cool companion (e.g. a cool WD) requires $M_2 \sin i > 1$ M$_\odot$ (Maoz et al. 2015) and can be ruled out. Modulation due to reflection of the WD light by a giant planet is also unlikely since the planet would be marginally within the WD's tidal radius for its density. The relatively high upper limit on the possible companion effective temperature (≈2500 K), does not allow us to rule out reflection or re-radiation from a brown dwarf companion. A remaining possible explanation for the optical modulations is rotation combined with a non-uniform accretion of the metals that we have, in fact, detected in the UV spectrum of this WD.

In the case of WD J1857+4909, a massive ≈1 M$_\odot$ WD, we can place an upper limit of $M_2 \sin i \lesssim 0.19$ M$_\odot$ on any companion based on the 2.2 h orbital period. This is only marginally consistent with a beaming explanation as the cause for the optical variations, as beaming would require $M_2 \sin i > 0.25$ M$_\odot$ (Maoz et al. 2015). Østensen et al. (2011) have suggested unresolved Zeeman splitting from a weak magnetic field as the cause for the line broadening in the optical spectrum of this WD. The atmospheric fit tends to overestimate the mass in the presence of unresolved Zeeman splitting, but the mass would still be relatively high. Reflection from a giant planet is not a viable solution because such a planet's orbit would be well within the WD's tidal disruption radius. A brown dwarf companion with a very high albedo could marginally have a low enough effective temperature to satisfy the $T_{\rm eff} < 1000$ K limit from the SED, while producing the optical modulation via reflection of the WD light. Since no metals are detected, within our sensitivity limits, in the photosphere of this WD, there is no evidence for modulation that is associated with an uneven photospheric distribution of accreted metals, combined with rotation.

WD 2359−434 has $M \approx 0.85$ M$_\odot$, and RV measurements using the narrow Hα NLTE absorption line core were made by Maxted & Marsh (1999). When folded over the observed period, these show no significant RV variations (Gary et al. 2013) down to ≈20 km s^{-1}, implying $M_2 \sin i \lesssim 45$ M$_{\rm Jup}$, i.e. the RV data do not rule out a cool (<1000 K, from the SED constraints, above) brown dwarf companion. However, the variability in this cool ($T_{\rm eff} \approx 8600$ K) and hence likely convective-atmosphere WD could simply be the result of star spots combined with rotation (but see Section 3.2.3 for a possible conflict of this picture with the observed UV spectrum).

5 DISCUSSION AND CONCLUSIONS

We have obtained *HST* UV spectra of seven WDs in order to test for a connection between debris accretion and periodic optical variability. The results of our experiment, and especially the presence of metal absorption lines in non-variable WDs, indicate that our null hypothesis, that optical variability and debris accretion are not directly linked, cannot be rejected. The cause of low-level periodic variability in a large fraction of WDs remains unclear. However, despite the results of our experiment, rotation combined with an

[6] http://www.astro.umontreal.ca/~bergeron/CoolingModels/

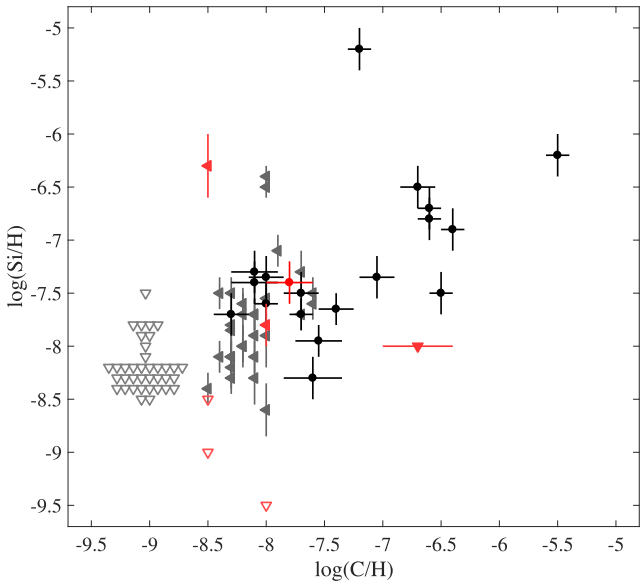

Figure 9. Si and C abundances relative to H, in the Koester et al. (2014) sample (grey-scale symbols), and in our sample (red). Actual detections are represented by errorbars along the appropriate dimension, while upper limits are represented by triangle-shaped symbols. For WD's with only upper limits on log (Si/H), no upper limits were reported by Koester et al. (2014) for log (C/H), so we plot them at an arbitrary log (C/H) = −9, with some small scatter added to avoid clutter in the figure. The upper limits in the Koester et al. (2014) sample are at abundance values similar to those of the actual detections, suggesting that a larger fraction of the sample, perhaps approaching 100 per cent, might reveal photospheric metals at similar abundances, if observed at higher sensitivity.

inhomogeneous atmospheric metal distribution could still be the mechanism behind the variability in some or all cases. Fig. 8 of Koester et al. (2014) shows that, in many WD with UV spectroscopy, the upper limits on Si abundance are comparable to the levels of the actual detections in other WDs. Metals at similar abundance levels could therefore be present in most or even all WDs. To illustrate this, we re-plot in Fig. 9 both the Si and C abundances, or upper limits thereof, for the Koester et al. (2014) WD sample, as tabulated by them, and add the measurements and upper limits from this work. In our sample, in the variable, but 'metal free', WDs, the metal abundances could be non-zero but simply below the limits that our observations are sensitive to.

Looking back at the atmospheric parameters of the WDs in our sample (Table 2), it appears that all of the non-variable WDs have 'normal' parameters of $\log g \sim 8$ and a non-convective effective temperature, while each of the variable WDs is somewhat abnormal: WD J1855+4207 has a relatively low mass that might indicate binarity (or at least a binary past), WD J1857+4909 is massive with some indication of a moderate magnetic field, and WD 2359−434 is magnetic and possibly convective. The determining factor linking debris accretion to optical variability could thus be the strength of a magnetic field such that accretion can be channelled inhomogeneously over the WD surface. Alternatively, magnetic fields might be behind the WD surface inhomogeneity of variable WDs, but without the intercession of photospheric metals. Subtle magnetic-field-sensitive radiative-transfer effects might exist, that when combined with rotation, could produce the low, $\sim 10^{-4}$, observed photometric modulation levels.

Our observations include two cases of photospherically polluted hot WDs that show high-ionization lines from apparently circumstellar material that is perhaps infalling, or alternatively, in a layer not far above the photosphere, such that the lines have velocities similar to, or slightly blue-shifted compared to the gravitationally redshifted photospheric lines. The two WDs are similar in this aspect to several others recently reported (see Section 3.2.1). The circumstellar material, if that is indeed its nature, may provide a new and important perspective on WD debris accretion.

More sensitive observations are required to resolve the puzzle of periodic optical variability. Deeper UV spectra could reveal up to what degree photometric metals are actually ubiquitous in WDs. Higher resolution optical spectroscopy can set firmer constraints on, or reveal, binary companions inducing the optical modulation. Such high-resolution spectra could also illuminate the connection, if one exists, to magnetic field strength.

ACKNOWLEDGEMENTS

We thank Gilles Fontaine for his help with the modelling of J1926+4219. We thank our contact scientist, Cristina Oliveira, and our programme coordinator, Amber Armstrong, at the Space Telescope Science Institute (STScI), for their help in carrying out the observations. NH thanks Elaine Snyder from the COS Team Help Desk for her help with the CALCOS pipeline, Siyi Xu for her help with TLUSTY, and Yossi Shvartzvald and Eran Ofek for their help with the *Spitzer* data. The anonymous referee is thanked for valuable comments. Based on observations made with the NASA/ESA *Hubble Space Telescope*, obtained at the Space Telescope Science Institute, which is operated by the Association of Universities for Research in Astronomy, Inc., under NASA contract NAS 5-26555. These observations are associated with programmes 14082 (PI: Maoz), 11526 (PI: Green), and 14076 (PI: Gänsicke). Support for programme 14082 was provided by NASA through a grant from the Space Telescope Science Institute, which is operated by the Association of Universities for Research in Astronomy, Inc., under NASA contract NAS 5-26555. Based on observations obtained at the MMT Observatory, a joint facility of the Smithsonian Institution and the University of Arizona, and on observations obtained with the Apache Point Observatory 3.5 m telescope, which is owned and operated by the Astrophysical Research Consortium. This work was supported by Grant 648/12 of the Israel Science Foundation (ISF) and by Grant 1829/12 of the Israeli Centers for Research Excellence (I-CORE) programme of the Planning and Budgeting Committee (PBC) and the ISF. The research leading to these results has received funding from the European Research Council under the European Union's Seventh Framework Programme (FP/2007-2013) / ERC grant agreement no. 320964 (WDTracer). This research has made use of the VizieR catalogue access tool, CDS, Strasbourg, France. This work is based in part on observations made with the *Spitzer Space Telescope*, obtained from the NASA/IPAC Infrared Science Archive, both of which are operated by the Jet Propulsion Laboratory, California Institute of Technology under a contract with the National Aeronautics and Space Administration. This work used the astronomy and astrophysics package for MATLAB (Ofek 2014).

REFERENCES

Abgrall H., Roueff E., Launay F., Roncin J. Y., Subtil J. L., 1993, A&AS, 101, 273

Allard F., 2016, in Reylé C., Richard J., Cambrésy L., Deleuil M., Pécontal E., Tresse L., Vauglin I., eds, SF2A-2016: Proc. Annu. Meeting French Soc. Astron. Astrophys. p. 223

Althaus L. G., Córsico A. H., Isern J., García-Berro E., 2010, A&A Rev., 18, 471
Angel J. R. P., Borra E. F., Landstreet J. D., 1981, ApJS, 45, 457
Asplund M., Grevesse N., Sauval A. J., Scott P., 2009, ARA&A, 47, 481
Aznar Cuadrado R., Jordan S., Napiwotzki R., Schmid H. M., Solanki S. K., Mathys G., 2004, A&A, 423, 1081
Barstow M. A., Boyce D. D., Welsh B. Y., Lallement R., Barstow J. K., Forbes A. E., Preval S., 2010, ApJ, 723, 1762
Borucki W. J. et al., 2010, Science, 327, 977
Brinkworth C. S., Marsh T. R., Morales-Rueda L., Maxted P. F. L., Burleigh M. R., Good S. A., 2005, MNRAS, 357, 333
Brown W. R., Gianninas A., Kilic M., Kenyon S. J., Allende Prieto C., 2016, ApJ, 818, 155
Chayer P., Vennes S., Pradhan A. K., Thejll P., Beauchamp A., Fontaine G., Wesemael F., 1995, ApJ, 454, 429
Chayer P., Kruk J. W., Ake T. B., Dupree A. K., Malina R. F., Siegmund O. H. W., Sonneborn G., Ohl R. G., 2000, ApJ, 538, L91
Debes J. H., Kilic M., Faedi F., Shkolnik E. L., Lopez-Morales M., Weinberger A. J., Slesnick C., West R. G., 2012, ApJ, 754, 59
Doyle T. F., Howell S. B., Petit V., Lépine S., 2017, MNRAS, 464, 3464
Farihi J., Gänsicke B. T., Koester D., 2013, Science, 342, 218
Fontaine G., Brassard P., Bergeron P., 2001, PASP, 113, 409
Fontaine G., Green E., Brassard P., Latour M., Chayer P., 2014, in van Grootel V., Green E., Fontaine G., Charpinet S., eds, ASP Conf. Ser. Vol. 481, 6th Meeting on Hot Subdwarf Stars and Related Objects. Astron. Soc. Pac., San Francisco, p. 83
Fulton B. J. et al., 2014, ApJ, 796, 114
Gänsicke B. T., Koester D., Farihi J., Girven J., Parsons S. G., Breedt E., 2012, MNRAS, 424, 333
Gary B. L., Tan T. G., Curtis I., Tristram P. J., Fukui A., 2013, Soc. Astron. Sci. Annu. Symp., 32, 71
Gentile Fusillo N. P., Tremblay P.-E., Jordan S., Gänsicke B. T., Kalirai J. S., Cummings J., 2018, MNRAS, 473, 3693
Giammichele N., Bergeron P., Dufour P., 2012, ApJS, 199, 29
Girven J., Gänsicke B. T., Steeghs D., Koester D., 2011, MNRAS, 417, 1210
Green J. C. et al., 2012, ApJ, 744, 60
Greenstein J. L., Oke J. B., 1979, ApJ, 229, L141
Heber U., 2016, PASP, 128, 082001
Hermes J. J. et al., 2017, ApJS, 232, 23
Hubeny I., 1988, Computer Phys. Commun., 52, 103
Hubeny I., Lanz T., 1995, ApJ, 439, 875
Hubeny I., Lanz T., 2011, Synspec: General Spectrum Synthesis Program. Astrophysics Source Code Library, record ascl:1109.022
Hubeny I., Lanz T., 2017a, preprint (arXiv:1706.01859)
Hubeny I., Lanz T., 2017b, preprint (arXiv:1706.01937)
Jura M., 2003, ApJ, 584, L91
Kawka A., Vennes S., Schmidt G. D., Wickramasinghe D. T., Koch R., 2007, ApJ, 654, 499
Kilic M., von Hippel T., Leggett S. K., Winget D. E., 2006, ApJ, 646, 474
Koester D., 2009, A&A, 498, 517
Koester D., Wilken D., 2006, A&A, 453, 1051
Koester D., Weidemann V., Zeidler-K. T. E. M., Vauclair G., 1985, A&A, 142, L5
Koester D., Dreizler S., Weidemann V., Allard N. F., 1998, A&A, 338, 612
Koester D., Voss B., Napiwotzki R., Christlieb N., Homeier D., Lisker T., Reimers D., Heber U., 2009, A&A, 505, 441
Koester D., Gänsicke B. T., Farihi J., 2014, A&A, 566, A34
Kuchner M., Burrows A., Reach W., Winget D., von Hippel T., 2004, Survey for Planets and Exozodiacal Dust Around White Dwarfs, Spitzer Proposal
Lallement R., Welsh B. Y., Barstow M. A., Casewell S. L., 2011, A&A, 533, A140
Landstreet J. D., Bagnulo S., Valyavin G., Valeev A. F., 2017, A&A, 607, 15
Long K. S., Gilliland R. L., 1999, ApJ, 511, 916
Makovoz D., Marleau F. R., 2005, PASP, 117, 1113
Manser C. J. et al., 2016, MNRAS, 455, 4467
Maoz D., Hallakoun N., 2017, MNRAS, 467, 1414
Maoz D., Mazeh T., McQuillan A., 2015, MNRAS, 447, 1749
Maoz D., Hallakoun N., Badenes C., 2018, MNRAS, in press, preprint (arXiv:1801.04275)
Maxted P. F. L., Marsh T. R., 1999, MNRAS, 307, 122
Mullally F., Kilic M., Reach W. T., Kuchner M. J., von Hippel T., Burrows A., Winget D. E., 2007, ApJS, 171, 206
Nelan E. P., Wegner G., 1985, ApJ, 289, L31
Ochsenbein F., Bauer P., Marcout J., 2000, A&AS, 143, 23
Ofek E. O., 2014, MATLAB Package for Astronomy and Astrophysics. Astrophysics Source Code Library, record ascl:1407.005
Pinto P. A., Eastman R. G., 2000, ApJ, 530, 757
Reach W. T. et al., 2005, PASP, 117, 978
Shvartzvald Y. et al., 2016, MNRAS, 457, 4089
Sion E. M., Cheng F. H., Szkody P., Sparks W., Gänsicke B., Huang M., Mattei J., 1998, ApJ, 496, 449
Steele P. R., Burleigh M. R., Dobbie P. D., Jameson R. F., Barstow M. A., Satterthwaite R. P., 2011, MNRAS, 416, 2768
Tremblay P.-E., Bergeron P., 2009, ApJ, 696, 1755
Tremblay P.-E., Fontaine G., Freytag B., Steiner O., Ludwig H.-G., Steffen M., Wedemeyer S., Brassard P., 2015, ApJ, 812, 19
Wegner G., 1982, ApJ, 261, L87
Werner M. et al., 2012, Small SpiKeS: Small Spitzer Kepler Survey, Spitzer Proposal
Werner M. et al., 2013, SpiKeS: Spitzer Kepler Survey, Spitzer Proposal
Winn J. N., Fabrycky D. C., 2015, ARA&A, 53, 409
Xu S., Jura M., Koester D., Klein B., Zuckerman B., 2013, ApJ, 766, L18
Xu S., Zuckerman B., Dufour P., Young E. D., Klein B., Jura M., 2017, ApJ, 836, L7
Zucker S., Mazeh T., Alexander T., 2007, ApJ, 670, 1326
Zuckerman B., Koester D., Reid I. N., Hünsch M., 2003, ApJ, 596, 477
Zuckerman B., Melis C., Klein B., Koester D., Jura M., 2010, ApJ, 722, 725
Zuckerman B., Xu S., Klein B., Jura M., 2013, ApJ, 770, 140
Østensen R. H. et al., 2010, MNRAS, 409, 1470
Østensen R. H. et al., 2011, MNRAS, 414, 2860

This paper has been typeset from a TEX/LATEX file prepared by the author.